Heliyon 10 (2024) e24575

Contents lists available at ScienceDirect

Heliyon

journal homepage: www.cell.com/heliyon

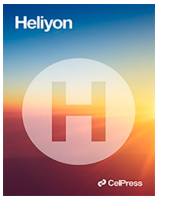

Research article

Huc-MSC-derived exosomal miR-144 alleviates inflammation in LPS-induced preeclampsia-like pregnant rats via the FosB/Flt-1 pathway

Jingchi Sun [a,b], Weishe Zhang [b,c,*]

[a] Department of Medical Administration, The Third People's Hospital of Chengdu, Chengdu, 610014, China
[b] Department of Obstetrics, Xiangya Hospital, Central South University, Changsha, 410008, China
[c] Hunan Engineering Research Center of Early Life Development and Disease Prevention, Changsha, 410008, China

ARTICLE INFO

Keywords:
Preeclampsia
FosB
miR-144
Exosomes
Flt-1

ABSTRACT

Background: Preeclampsia (PE) is a common and severe hypertensive disorder in pregnancy. Mesenchymal stem cell-derived exosomes (Exos-MSC) have been reported to mitigate the progression of inflammatory diseases. The study aimed to explore the effects of human umbilical cord-derived Exos-MSC (huc-Exos-MSC) on PE-like models.

Methods: Lipopolysaccharide (LPS) was used to construct *in vitro* and *in vivo* PE-like models. Exosomes were treated with LPS-induced PE-like cells and rats.

Results: PE-like inflammatory models of pregnant rats and cells were successfully constructed *in vivo* and *in vitro*. miR-144 was screened by bioinformatics analysis. Exosomes were successfully extracted. Silencing FosB, overexpressing miR-144 or treating with exosomes extracted from huc-MSC overexpressing miR-144 in (Exos-MSC$^{miR-144}$) reversed the LPS-induced decline in HTR-8/SVneo cell viability and migration. In addition, the above groups decreased LPS-induced increases in interleukin 6 (IL-6), tumor necrosis factor-α (TNF-α), phosphorylated nuclear factor-kappaB (p–NF–κB)/NF-κB, soluble FMS-like tyrosine kinase 1 (sFlt-1), and Flt-1 levels. Simultaneously, transfection of miR-144 mimics and overexpressing FosB reversed those changes in the miR-144 mimics group. miR-144 might alleviate LPS-induced HTR-8/SVneo cell inflammation by targeting FosB. Injection of Exos-MSC$^{miR-144}$ in PE-like pregnant rats reversed LPS-induced increases in FosB expression, systolic and diastolic blood pressure (SBP and DBP), as well as mean arterial pressure (MAP), heart rate, urine albumin/creatine ratio, inflammatory factors, p–NF–κB/NF-κB, and sFlt-1 levels. Furthermore, compared with the model group, the proportion of live births was significantly higher in the model + Exos-MSC$^{miR-144}$ group, while the apoptosis rate of fetal rat brain tissue was significantly lower.

Conclusions: We found that huc-Exos-MSC-derived miR-144 alleviated gestational hypertension and inflammation in PE-like pregnant rats by regulating the FosB/Flt-1 pathway. In addition, huc-Exos-MSC-derived miR-144 could partially reverse the LPS-induced adverse pregnancy outcome and brain injury in fetal rats, laying the foundation for developing new treatments for PE.

* Corresponding author. Department of Obstetrics, Xiangya Hospital, Central South University, 87 Xiangya Road, Changsha, 410008, China.
E-mail address: zhangweishe@yeah.net (W. Zhang).

https://doi.org/10.1016/j.heliyon.2024.e24575
Received 27 April 2023; Received in revised form 21 December 2023; Accepted 10 January 2024
Available online 17 January 2024

1. Introduction

Preeclampsia (PE) is estimated to affect 2–8% of pregnancies worldwide. This disease is the main cause of maternal and fetal mortality [1]. The main pathological features of PE are placental hypoxia-ischemia, inflammation, oxidative stress, vascular and endothelial cell dysfunction, etc., and these features eventually lead to a range of clinical symptoms such as hypertension, proteinuria, headaches and other systemic dysfunctions [2]. At present, the only confirmed treatment for PE is to deliver the fetus [3]. It is urgent for us to study the pathogenesis of PE further.

In clinical studies, soluble FMS-like tyrosine kinase 1 (sFlt-1) can be used as a potential marker of PE and has been reported many times [4–7]. It has been proven that miR-139–5p promotes the proliferation and invasion of trophoblast cells by directly targeting sFlt-1 in PE [4]. Other studies have shown that inhibition of sFlt1 by the JNK/AP-1 pathway may be a potential pathway to prevent PE [5]. The AP-1 family consists of the Fos family and JUN family heterodimers, including Fos, FosB, Fos-like antigen 1 (FosL1), FosL2, Jun, JunB and JunD. They may be involved in the development of PE [5,8,9]. FosB has been proven to be closely related to PE, but its specific mechanism has not been studied in depth [10]. To the best of our knowledge, the regulatory mechanism of miRNA by targeting AP-1 has not been reported in PE. AP-1 is closely related to depression, Parkinson's disease and other neurological diseases [11,12]. We speculated that regulating its pathways might affect fetal brain development through placental tissue.

Mesenchymal stem cells (MSCs) have immunomodulatory properties and have been shown to have the potential to treat a variety of diseases, including PE [13,14]. The potential benefits of human umbilical cord-derived MSCs (huc-MSCs) may be due to interference with pathogenic immune responses and paracrine cell protection [15]. *In vivo*, huc-MSC-derived exosomes (huc-Exos-MSC) can improve the morphology of placental tissue in PE rats in a dose-dependent manner by inhibiting cell apoptosis and promoting placental tissue angiogenesis [16]. MicroRNAs (miRNAs) are a class of noncoding, single-stranded RNAs consisting of 19–25 nucleotides [17]. miRNA dysregulation and its potential functions have been important directions in elucidating the mechanisms of PE [18]. For example, miR-30-5p-mediated ferroptosis of trophoblast cells has been implicated in the pathogenesis of PE [19]. miR-4443 inhibits trophoblast migration and invasion in PE [18]. Extracellular vesicles (EVs) at least partially mediate paracrine activity. MSC-derived EVs can mimic the functions of parental MSCs by transferring their components, including miRNA, to recipient cells [20]. Exos-MSC can relieve myocardial ischemia-reperfusion, osteoarthritis, intervertebral disc degeneration and other diseases by transporting miR-182, miR-92a-3p, miR-21, etc. [21–23]. In related studies on PE, *in vitro* studies have shown that miR-133b derived from Exos-MSC can promote the proliferation, migration and invasion of HTR8/SVneo cells in PE by inhibiting SGK1 [24]. However, whether there are miRNAs in Exos-MSC that regulate AP-1-related pathways in PE is not clear and is worthy of further study.

This research explores the potential mechanism of Exos-MSC in the treatment of PE-like models *in vivo* and *in vitro* and the effects on neuronal apoptosis in neonatal rats of eclampsia pregnant rats. We hope that this research will lay the foundation for the development of new methods for clinical diagnosis and treatment.

2. Materials and methods

2.1. Cell treatment

HTR-8/SVneo cells (ZQ0482), commonly used in experiments as human villus trophoblast cells, were purchased from Zhongqiao Xinzhou (Shanghai, China). The cells were routinely cultured in a 37 °C incubator. The cells were processed according to the following two protocols. After reaching the predetermined time, the cells were collected. Each experiment was repeated at least three times.

Protocol one was as follows:

(i) Control: The cells were treated with the same volume of solvent (phosphate buffer saline) in the lipopolysaccharide (LPS) group for 48 h (ii) LPS: The cells were treated with 100 ng/mL LPS for 48 h [5,8]. (iii) LPS + negative control of silencing FosB (NC si-FosB): The cells were treated with 100 ng/mL LPS and simultaneously transfected with the NC of the si-FosB plasmid. (iv) LPS + si-FosB: The cells were transfected with si-FosB plasmid while being treated with 100 ng/mL LPS.

Protocol two was as follows:

(i) LPS: The cells were treated the same as above. (ii) mimics-NC: The cells were treated with 100 ng/mL LPS and simultaneously transfected with the NC of miR-144 mimics. (iii) miR-144 mimics: The cells were treated with 100 ng/mL LPS and simultaneously transfected with miR-144 mimics. (iv) miR-144 mimics + overexpression-NC (oe-NC): The cells were treated with 100 ng/mL LPS and simultaneously transfected with the NC of the oe-FosB plasmid. (v) miR-144 mimics + oe-FosB: The cells were transfected with oe-FosB plasmid and treated with 100 ng/mL LPS.

2.2. Extraction and uptake of Exos-MSC

The huc-MSCs (cat# CP-CL11) were purchased from Pricella Biotech (Wuhan, Hubei, China). The cells were cultured in a 37 °C incubator. The cells were cultured in a serum-free medium for 72 h. The exosomes were extracted from the cell culture medium according to the instructions of the exosomes extraction kit (4,478,359, Thermo Fisher, USA) as described previously [25]. Briefly, the supernatants from the collected cultures were centrifuged at 2000×*g* for 10 min to remove cellular debris and vesicles. They were then subjected to a second round of centrifugation at 10,000×*g* for 20 min. The resultant pellet contained exosomes, which were further extracted through ultracentrifugation at 110,000×*g* for 70 min and subsequently washed with PBS using the same ultracentrifugation conditions. Finally, the purified exosomes were resuspended in PBS. The BCA Protein Assay Kit (Thermo Fisher Scientific, USA) was utilized to quantify the exosomal proteins. The morphologic pictures of Exos-MSC were obtained via transmission electron microscopy

(TEM), as previously reported [26]. The particle size of exosomes were measured by nanoparticle tracking analysis (NTA), as previously reported [27]. Exosomes were labeled with PKH26 (PKH26PCL, Sigma, Germany) and subsequently utilized to treat the HTR-8/SVneo cells for 12 h. The uptake of exosomes in HTR-8/SVneo cells was observed by confocal fluorescence microscopy (BA210T, Motic).

2.3. Treatment of Exos-MSC

The huc-MSCs were divided into 4 groups and treated according to protocol three.

Protocol three was as follows:

(i) MSC-NC: MSCs were transfected with the negative control plasmid of miR-144 mimics for 48 h (ii) MSC-miR-144: MSCs were transfected with miR-144 mimics for 48 h (iii) Exos-MSC^{NC}: exosomes extracted from the cells of the MSC-NC group; (iv) Exos-MSC$^{miR-144}$: exosomes extracted from the cells of the MSC-miR-144 group.

The exosomes obtained above were derived from huc-MSCs transfected with NC or miR-144 mimics, and HTR-8/SVneo cells were processed according to protocol four.

Protocol four was as follows:

(i) LPS: The HTR-8/SVneo cells were treated with 100 ng/mL LPS for 48 h as described above. (ii) LPS + Exos-MSC^{NC}: At the same time as LPS treatment, 1.3×10^5 particles/cell exosomes from the MSC-NC group were used to treat the HTR-8/SVneo cells for 48 h [28,29]. (iii) LPS + Exos-MSC$^{miR-144}$: At the same time as the LPS treatment, 1.3×10^5 particles/cell exosomes from the MSC–NC–miR-144 group were used to treat the HTR-8/SVneo cells for 48 h.

2.4. Animal treatment

Sprague-Dawley (SD) rats (10–12 weeks, 280–330 g) were purchased from Hunan SJA Laboratory Animal Co., Ltd (Hunan, China). The rats were free to drink water and obtain food at (25 ± 2) °C with 12 h/12 h alternating day and night. To ensure that pregnant rats remained quiet during blood pressure measurement, female rats were trained to comply with caudate artery blood pressure measurements every day, and adaptive culture lasted for a week. The experiment was approved by the Central South University Animal Welfare Ethics Committee (NO.202103402). Male and female rats were cultured in a 1:1 mixed cage overnight. Thereafter, the male rats were separated. If a vaginal plug was seen the next morning, it was recorded as Day 0 of gestation (GD0) for that rat. Pregnant rats were divided into 5 groups (n = 6 rats/group), including the Sham, Model, Model + Exo-MSC-low (Exosomes treatment at a low concentration of 7.8×10^9 particles/mL), Model + Exo-MSC-mid (Exosomes treatment at a middle concentration of 1.55×10^{10} particles/mL), and Model + Exo-MSC-high (Exosomes treatment at a high concentration of 3.1×10^{10} particles/mL) groups [16,30], to explore the optimal concentration for exosome treatment.

Then, pregnant rats were further randomly divided into four groups on the GD14 (n = 10 rats/group). (i) Sham: sterile normal saline of the same volume as the model group was slowly injected into the tail vein of normally pregnant rats on the GD14, and a microinjection pump was used to control the speed. In addition, sterile saline was injected intraperitoneally as described for the Model + Exos-MSC$^{miR-144}$ group. (ii) Model: To establish a PE-like animal model, on the GD14, LPS (1 μg/kg) was injected into the tail vein with the help of a microinjection pump [31,32]; Sterile saline was injected intraperitoneally as described for the Model + Exos-MSC$^{miR-144}$ group. (iii) Model + Exos-MSC^{NC}: As in the model group, the same dose of LPS was administered from the tail vein at the same time. However, pregnant rats were intraperitoneally injected with 3.1×10^{10} particles/mL exosomes suspension from the Exos-MSC^{NC} group at 0.5 mL/day for 6 days. (iv) Model + Exos-MSC$^{miR-144}$: Caudal vein injection was the same as the model group on the GD14. Pregnant rats were intraperitoneally injected with 3.1×10^{10} particles/mL exosomes suspension from the Exos-MSC$^{miR-144}$ group at 0.5 mL/day for 6 days. The blood pressure of pregnant rats in all four groups was measured every 2 or 3 days between 8:00 and 12:00. On the GD18, the urine of pregnant rats was collected in a metabolic cage for 24 h and frozen at −80 °C. Urine protein and creatinine levels were detected using a urine protein quantitative detection kit (A028-2-1, Nanjing, China) and a creatinine detection kit (C011-2-1, Nanjing, China). At GD20, 10 pregnant rats in each group were sacrificed. The weight of pregnant rats and the number of live and stillborn rats were recorded. Placental tissue, peripheral blood, and fetal brain were collected. The whole brains of fetal rats were fixed with 4 % paraformaldehyde for pathological evaluation. The remaining pregnant rats were sacrificed after giving birth naturally.

2.5. ELISA kits

The concentrations of interleukin 6 (IL-6), tumor necrosis factor-α (TNF-α), and sFlt-1 in the cells, cell supernatant, or serum of pregnant rats were measured, according to the manufacturer's instructions. IL-6 (human, CSB-E04638h; rat, CSB-E04640r; Cusabio Biotech, China), TNF-α (human, CSB-E04740h; rat, CSB-E11987r; Cusabio Biotech, China), and sFlt-1 (human, ml038123; rat, ml059017; Mlbio, China) kits were used. Briefly, the samples were pretreated and incubated with an antibody working solution or enzyme at 37 °C for 1 h. Afterward, the samples were incubated with horseradish peroxidase-labeled working solution for 1 h at 37 °C or color developer for 15 min at 37 °C protected from light. Finally, the optical density (OD) value of each well was obtained at 450 nm via a multifunction enzyme analyzer (MB-530, Heales, China).

2.6. Western blot

Total proteins in each group of cells, tissues or exosomes were extracted and then denatured. After SDS-gel electrophoresis, the proteins were transferred to nitrocellulose membranes. The primary antibodies were incubated overnight at 4 °C, including Flt-1 (1:500, 13687-1-AP, Proteintech, USA), FosB (1:10,000, ab184938, Abcam, UK), CD63 (1:500, 25682-1-AP, Proteintech, USA), HSP70 (1:10000, 10995-1-AP, Proteintech, USA), p–NF–κB (1:1000, ab183559, Abcam, UK), NF-κB (1:50,000, ab23536, Abcam, UK), Caspase3 (1:1000, 19677-1-AP, Proteintech, USA), and β-actin (1:5000, 66009-1-Ig, Proteintech, USA). Finally, they were incubated with the secondary antibody HRP goat anti-mouse IgG (1:5000, SA00001-1, Proteintech, USA) or HRP goat anti-rabbit IgG (1:6000, SA00001-2, Proteintech, USA) for 90 min at room temperature. β-actin was used as an internal control. After the ECL color exposure, the gel imaging system (ChemiScope6100, Shanghai Qinxiang, China) was used for imaging analysis. ImageJ software (National Institutes of Health, USA) was used to semiquantify the grayscale values of the immunoblots. The ratio of the gray value of the target protein to β-actin is the semiquantitative result.

2.7. Cell counting kit 8 (CCK8)

The cells processed above were tested for cell viability according to the instructions of the CCK8 detection kit (NU679, Dojindo, Japan) as described by previous authors [33]. In short, 10 % CCK8 was added to each well of cells. Then, after incubation at 37 °C for 2 h, the $OD_{450\ nm}$ value was detected.

2.8. Transwell

Petri dishes were supplemented with complete containing 10 % fetal bovine serum. Then, Transwell chambers (3428, Corning, USA) were placed into petri dishes. The treated cells (2×10^5 cells/mL) were used to seed the upper compartment. The cells were incubated at 37 °C for 48 h. After the upper chamber was removed, the cells in the upper chamber were wiped clean. After fixation, the cells were stained with crystal violet. Cell migration was observed under a microscope after decolorization. The $OD_{550\ nm}$ value was detected by the enzyme analyzer.

2.9. Quantitative real-time PCR (qRT-PCR)

Total RNA was extracted from tissues and cells according to the TRIzol specification (Invitrogen, USA). Then, the extracted RNA was reverse transcribed into cDNA. The target gene sequence was searched on NCBI, and primers were designed using Primer 5 software (Premier, BC). Primer sequences of each gene were as follows. Rat-FosB, sense 5′-ATGTTTCAAGCTTTCCCCGGAGACT-3′, antisense 5′-GCTGGTTGTGATTGCGGTGA-3′; Rat-Flt-1, sense 5′- CAGGACCATGCACCATAGCA-3′, antisense 5′-GCAGTGCTCACCTC-TAACGA-3’; Rat-miR-144, sense 5′- GGGCCTTGGCTGGGATATCAT-3′, antisense 5′- GGGGTACCCAGACTAGTACATCA-3′; Rat-5S, sense 5′- GCCTACAGCCATACCACCCGGAA-3′, antisense 5′- CCTACAGCACCCGGTATCCCA-3′; Rat-β-actin, sense 5′- ACATCCGTAAA-GACCTCTATGCC-3′, antisense 5′- TACTCCTGCTTGCTGATCCAC-3′; Human-FosB, sense 5′-GCTGCAAGATCCCCTACGAAG-3′, antisense 5′- ACGAAGAAGTGTACGAAGGGTT-3′; Human-Flt-1, sense 5′- TTTGCCTGAAATGGTGAGTAAGG-3′, antisense 5′-TGGTTTGCTTGAGCTGTGTTC-3’; Human-miR-144, sense 5′- TACAGTATAGATGATGTACT-3′; Human-U6, sense 5′-CTCGCTTCGGCAGCACA-3′, antisense 5′-AACGCTTCACGAATTTGCGT-3′; Human-β-actin, sense 5′- ACCCTGAAGTACCCCATCGAG-3′, antisense 5′- AGCACAGCCTGGATAGCAAC-3′. The relative expression levels of each target gene were calculated using $2^{-\Delta\Delta Ct}$ method with β-actin/5S/U6 as internal reference.

2.10. Bioinformatics analysis

The miRNA chip dataset GSE103542 was selected, including 16 PE and 8 Control samples. All data were normalized. The difference analysis R language limma package was applied. The cutoff was $|logFC|>log\ 2\ (1.5)$ and $p < 0.05$. Next, the interactions between the top six differentially downregulated miRNAs and FOS were selected and analyzed through DIANA Tools. The target predicted by hsa-miR-144 was subjected to Kyoto Encyclopedia of Genes and Genomes (KEGG) and Gene Ontology (GO) enrichment analysis. The enrichment analysis R language cluster profiler package was applied. $p < 0.05$ indicated a significant difference.

2.11. Dual-luciferase assay

The dual-luciferase assay was performed as previously described [34]. In brief, in a six-well plate, HEK-293A cells (AW-CNH216, Abiowell, Changsha, Hunan, China) were cultured to approximately 70 % confluence. The cells were subjected to the following four experiments. (i) The cells were cotransfected with pHG-MirTarget-FosB wild-type (WT) luciferase reporter vector (2 μg) and NC (50 nM). (ii) The cells were cotransfected with pHG-MirTarget-FosB WT luciferase reporter vector (2 μg) and miR-144 mimics (50 nM). (iii) The cells were cotransfected with pHG-MirTarget-FosB mutant (MUT) luciferase reporter vector (2 μg) and NC (50 nM). (iv) The cells

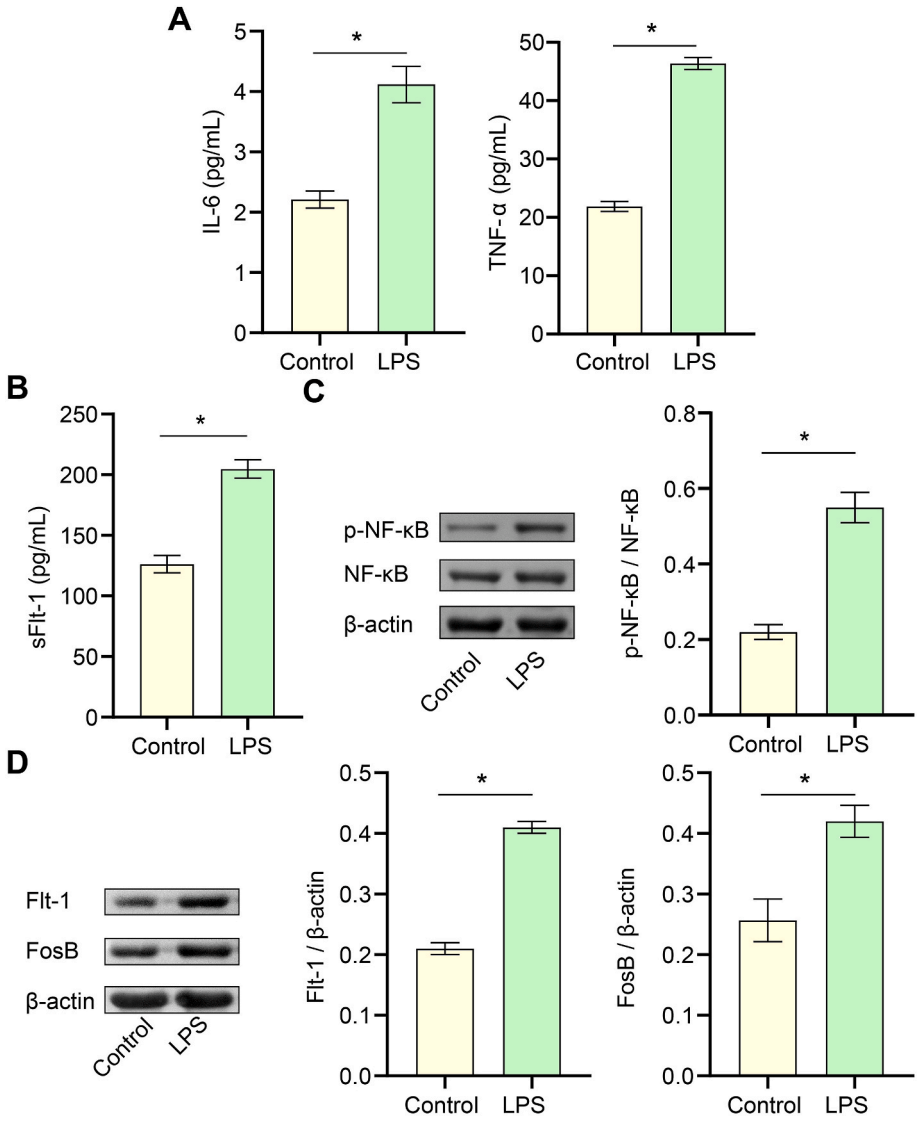

Fig. 1. LPS induced inflammation and activated the FosB/sFlt-1 pathway in HTR-8/SVneo cells. (A–B) The concentrations of IL-6, TNF-α, and sFlt-1 were detected by ELISA. (C) The protein expression levels of p–NF–κB and NF-κB were measured by Western blot. (D) The protein expression levels of Flt-1 and FosB were measured by Western blot. *$P < 0.05$. n = 3/group. The original immunoblots are available in Fig. S3. Each experiment was repeated at least three times.

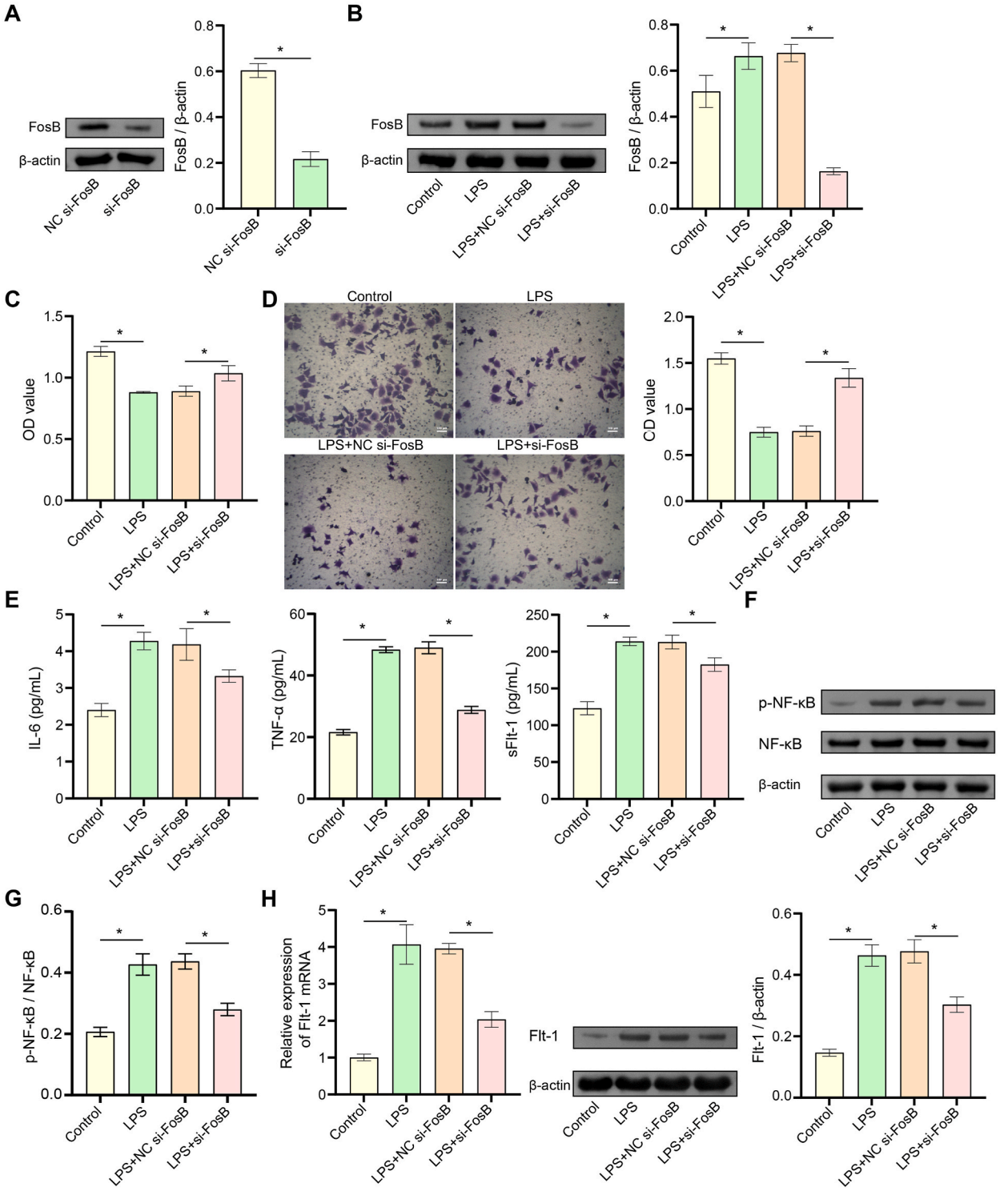

Fig. 2. Regulation of FosB/Flt-1 in LPS-induced HTR-8/SVneo cells. (A–B) The expression of FosB was detected by Western blot. (C) Cell viability of each group was detected by CCK8. (D) Cell migration was assessed by Transwell assays. (E) The levels of IL-6, TNF-α, and sFlt-1 were measured by ELISA. (F–G) The protein expression levels of p–NF–κB and NF-κB were measured by Western blot. (H) The Flt-1 expression was measured by qRT-PCR and Western blot. *$P < 0.05$. n = 3/group. The original immunoblots are available in Fig. S3. Each experiment was repeated at least three times.

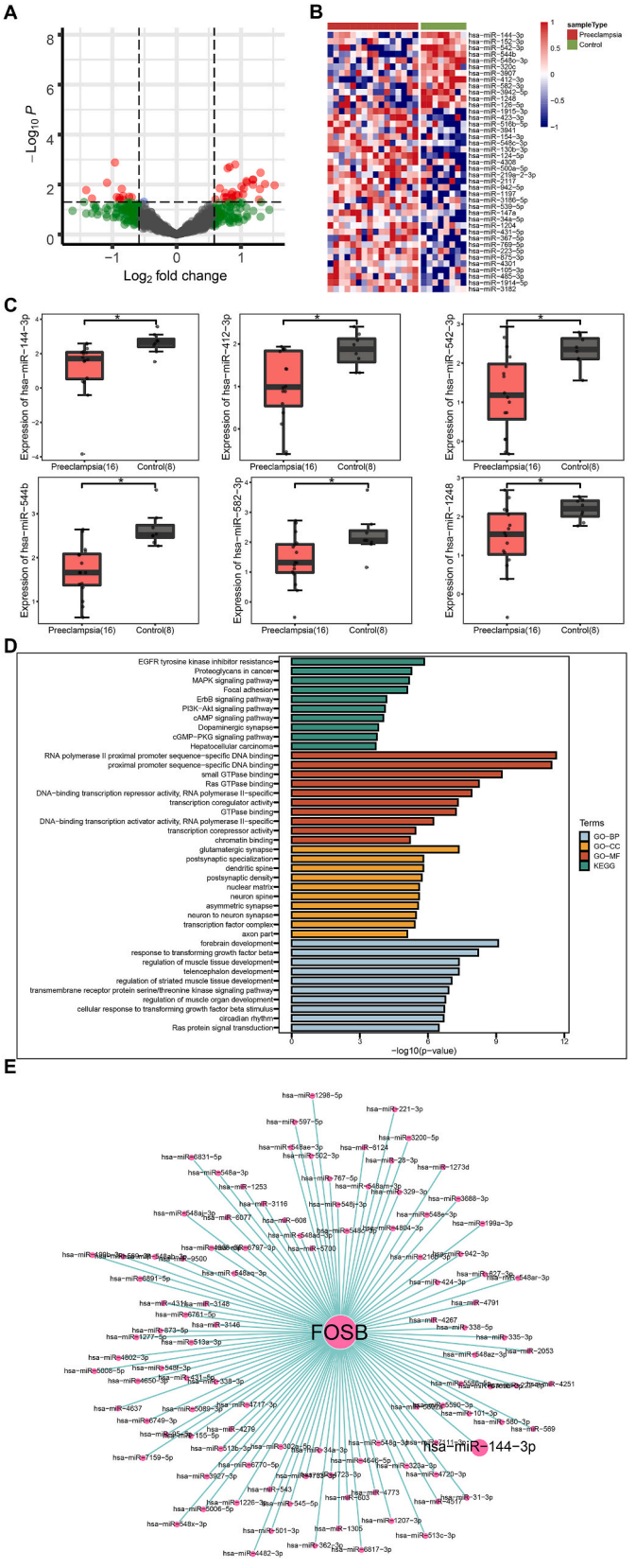

(caption on next page)

Fig. 3. Regulation of FosB candidate miRNA screening. (A–B) Volcano and heatmaps of miRNAs expressed significantly differently in PE. (C) Box plot of the top six miRNAs significantly downregulated in PE. (D) GO and KEGG enrichment analysis. (E) The potential miRNAs that might target FosB were predicted by dlana tools. *$P < 0.05$.

were cotransfected with pHG-MirTarget-FosB MUT luciferase reporter vector (2 μg) and miR-144 mimics (50 nM). Lipofectamine 2000 (2,028,090, Invitrogen, USA) was used to for cotransfection for 48 h. A dual-luciferase assay kit was purchased from Promega (E1910). After pretreatment, the cells were lysed for 15 min by adding 100 μL of 11xPLB lysate. LARII solution (100 μL) was added to the lysate, mixed and put into a luminescence detector (GloMax 20/20, Promega, USA) to detect the first luminescence (firefly luciferase activity). The first luminescence was terminated by adding 100 μL of Stop&Glo assay solution. The second luminescence value was detected (Reniera luciferase activity). The luciferase activity was normalized to Renilla luciferase activity.

2.12. Terminal deoxynucleotidyl transferase (TdT)-mediated dUTP nick end labeling (TUNEL) staining

The brain tissue sections of G20-day fetal rats were fixed in 4 % paraformaldehyde. TUNEL staining was performed, as previously described to measure neuronal apoptosis [35]. Briefly, the sections were treated with the TUNEL reaction mixture (40306ES50, YESEN Biotech, China), following the manufacturer's instructions. Representative images were viewed and analyzed through a fluorescence microscope and Image-Pro Plus (IPP) software.

2.13. Statistical analysis

Statistical analysis was performed using GraphPad Prism 9.0 software (GraphPad Software, USA). An unpaired *t*-test was used to determine statistical significance between the two groups. Three groups or more were determined by one-way analysis of variance, and then Tukey's HSD post hoc test was performed. The data are expressed as the mean ± standard deviation. *P value < 0.05 indicated a significant difference.

3. Results

3.1. LPS induced HTR-8/SVneo cell inflammation and activated the FosB/sFlt-1 pathway

LPS was used to stimulate HTR-8/SVneo cells to construct the PE-like model. The results showed that LPS stimulation could induce the release of IL-6, TNF-α, and sFlt-1 (Fig. 1A and B). The ratio of p–NF–κB/NF-κB rose after LPS stimulation (Fig. 1C). FosB is one of the main members of the AP-1 family and might be involved in the development of PE [8]. Therefore, the expression of FosB was detected by Western blot. The results showed that the expression of sFlt1 and FosB increased significantly after LPS stimulation (Fig. 1D). The above results suggested that the increased expression of FosB might be related to HTR-8/SVneo cell inflammation.

3.2. Silencing FosB might inhibit LPS-induced HTR-8/SVneo cells functional damage in regulating Flt-1

To further verify the mechanism by which FosB affects the inflammation of HTR-8/SVneo cells, the cells were transfected with si-FosB and the corresponding NC control. The results showed that the expression of FosB was significantly reduced after transfection of si-FosB, indicating that the transfection was successful (Fig. 2A). Western blot results showed that compared with the LPS + NC si- FosB group, the expression of FosB in the LPS + si-FosB group was reduced (Fig. 2B). The results showed that silencing FosB significantly reversed the decrease in the cell viability, the cell migration speed, and the concentration of IL-6, TNF-α, and sFlt-1 caused by LPS stimulation (Fig. 2C–E). FosB silencing significantly reduced the expression of LPS-stimulated p–NF–κB/NF-κB and Flt-1 levels (Fig. 2F–H). These results suggested that silencing FosB might inhibit LPS-induced HTR-8/SVneo cells dysfunction by regulating Flt-1.

3.3. miR-144 might inhibit LPS-induced HTR-8/SVneo cell activity by targeting FosB

The miRNA regulatory network plays an important role in PE [36]. To further explore whether there is a corresponding miRNA regulating FosB in PE, we conducted a bioinformatics analysis through the GSE103542 database. The volcano map and heatmap results showed that compared with the control group, 12 miRNAs were significantly downregulated and 29 miRNAs were significantly upregulated in the placental tissue of PE (Fig. 3A and B). The top six miRNAs that were significantly downregulated in PE were miR-144, miR-412–3p, miR-542–3p, miR-544b, miR-582–3p, and miR-1248 (Fig. 3C). KEGG and GO results showed that the targeted mRNAs predicted by miR-144 were enriched in EGFR tyrosine kinase inhibitor resistance, proteoglycans in cancer, MAPK signaling pathway, RNA polymerase II proximal promoter sequence-specific DNA binding, proximal promoter sequence-specific DNA binding, and small GTPase binding and other pathways (Fig. 3D). Next, we predicted potential miRNAs that might target FosB by dlana tools, such as miR-144, miR-569, and miR-580. The only intersection of miRNAs differentially expressed in PE with potential miRNAs for FosB was miR-144 (Fig. 3E). Therefore, miR-144 was chosen for follow-up studies.

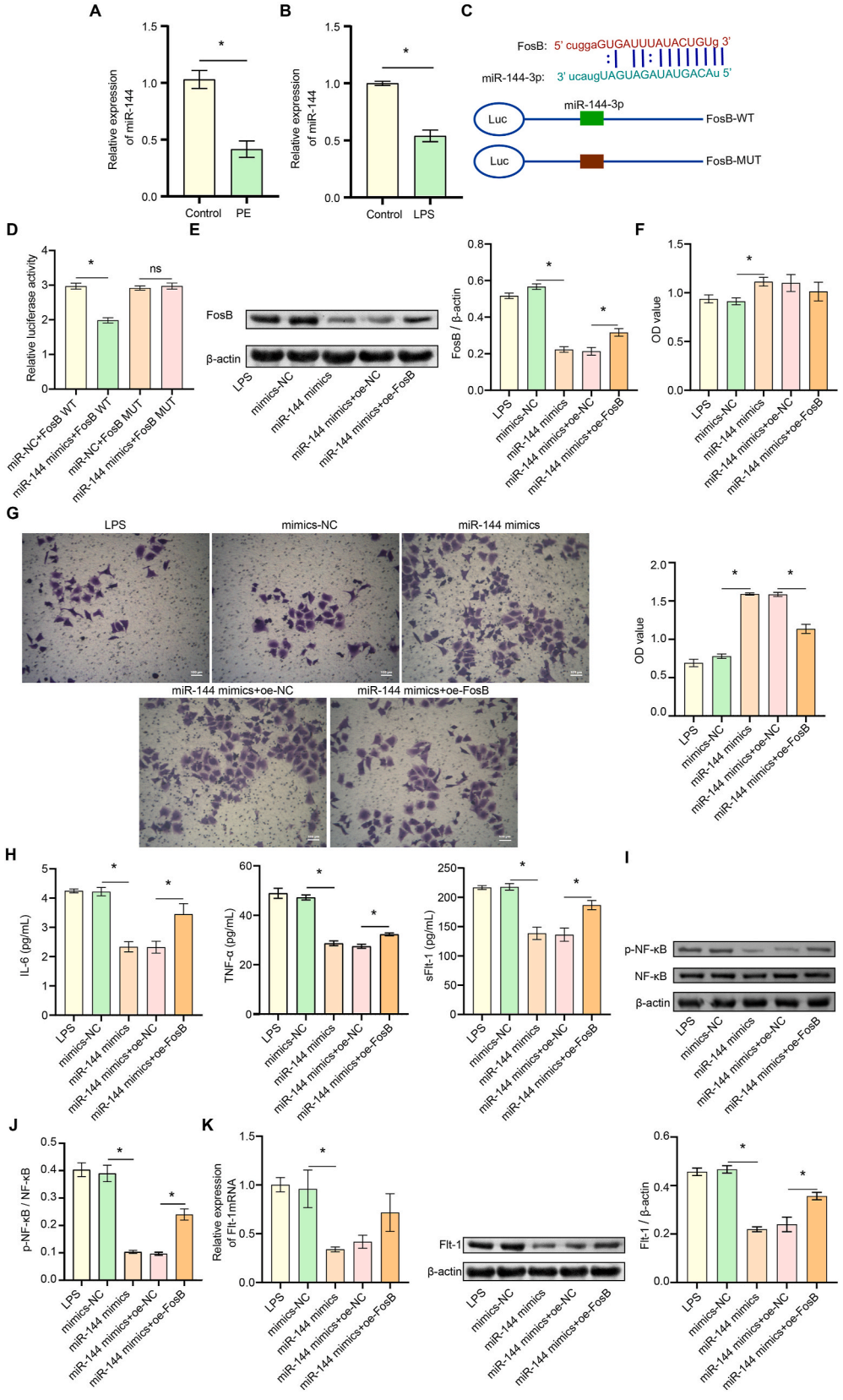

(caption on next page)

Fig. 4. miR-144 might inhibite LPS-induced HTR-8/SVneo cells activity by targeting FosB. (A) The expression of miR-144–3p in LPS-induced placental tissue of PE-like pregnant rats. (B) The expression of miR-144 was detected in LPS-induced HTR-8/SVneo cells. (C) The binding site map of miR-144 and FosB. (D) Dual-luciferase was used to detect the targeting relationship between miR-144 and FosB. (E) The expression of FosB was detected by Western blot. (F) Cell viability of each group was determined by CCK8. (G) Cell migration was assessed by Transwell. (H) The levels of IL-6, TNF-α, and sFlt-1 were measured by ELISA. (I–J) The expressions of p–NF–κB and NF-κB were measured Western blot. (K) The expressions of Flt-1 were measured by qRT-PCR and Western blot. $^{*}P < 0.05$. n = 3/group. The original immunoblots are available in Fig. S3. Each experiment was repeated at least three times.

To verify the above results, the expression of miR-144 in the placental tissue of PE-like pregnant rats and LPS-induced HTR-8/SVneo cells was tested. Consistent with the prediction results of bioinformatics analysis, the expression of miR-144 was downregulated in placental tissues and cells induced by LPS (Fig. 4A and B). Fig. 4C demonstrates the predicted target binding sites of miR-144 and FosB (Fig. 4C). The dual-luciferase results showed that, compared with the miR-NC + FosB WT group, the relative luciferase activity of the miR-144 mimics + FosB WT group decreased, suggesting that miRNA-144–3p targeted FosB (Fig. 4D).

Next, miR-144 was further overexpressed to explore its possible role in the LPS-induced cell model. The results showed that the expression of FosB in the miRNA-144 mimics group was significantly decreased compared with that in the mimic-NC group. In contrast to the miR-144 mimics + oe-NC group, the expression of FosB in the miR-144 mimics + oe-FosB group was significantly increased (Fig. 4E). After transfection with miR-144 mimics, the OD value and migration rate of cells were obviously improved. However, when transfected with miR-144 mimics and then transfected with oe-FosB, the OD value and migration rate showed a downward trend (Fig. 4F and G). The concentrations of IL-6, TNF-α, and sFlt-1, the ratio of p–NF–κB/NF-κB, and the expression of Flt-1 decreased significantly after transfection with miR-144 mimics. The miR-144 mimics + oe-FosB group reversed the above changes (Fig. 4H–K). Therefore, miR-144 might inhibite LPS-induced HTR-8/SVneo cell activity by targeting FosB.

3.4. *Exos-MSC$^{miR-144}$ might alleviate the functional damage of HTR-8/SVneo cells induced by LPS via inhibiting the FosB/Flt-1 pathway*

Exos-MSC have been reported to promote HTR-8/SVneo cell migration and invasion, but the specific mechanisms have not been thoroughly studied [37]. We extracted Exos-MSC. The morphology and diameter of the extracted exosomes were measured by TEM and NTA. The results showed that the exosomes had an oval vesicle-like structure with an average particle size of 134.1 nm (Figs. S1A–S1B). Western blot results reflected that CD63 and HSP70 were expressed in huc-MSCs and Exos-MSC, and the expression in MSCs was more obvious (Fig. S1C). The above results indicated that the exosomes were successfully extracted. The results of the exosomes uptake experiment indicated that HTR-8/SVneo cells could successfully take up exosomes (Fig. S1D).

First, different concentrations of exosomes (0, 3.25×10^4, 6.5×10^4, 1.3×10^5 and 2.6×10^5 particles/cell) were used to treat LPS-stimulated cells. The results showed that exosomes could promote the viability of cells in the model group in a concentration-dependent manner, and the exosome treatment at concentrations of 1.3×10^5 and 2.6×10^5 particles/cell had the most significant effect (Fig. S2A). Therefore, 1.3×10^5 particles/cell exosomes were chosen as the doses for cellular experimental treatments. To further explore whether the presence of miR-144 in exosomes affects the function of HTR-8/SVneo cells, first, huc-MSCs were transfected with empty or miR-144 mimics, and exosomes were extracted. The results showed that compared with that in the Exos-MSC^{NC} group, the expression of miR-144 in the Exos-MSC$^{miR-144}$ group increased significantly. The results of qRT−PCR showed that compared to the LPS group, the expression of miR-144 in the LPS + Exos-MSC^{NC} group and the LPS + Exos-MSC$^{miR-144}$ group was increased, and the latter expression was higher (Fig. 5A). The expression of FosB in the LPS + Exos-MSC^{NC} group and LPS + Exos-MSC$^{miR-144}$ group was significantly lower than that in the LPS group (Fig. 5B and C). Compared with those in the LPS + Exos-MSC^{NC} group, the cell viability and migration speed increased significantly in the LPS + Exos-MSC$^{miR-144}$ group, while the concentrations of IL-6, TNF-α, and sFlt-1, as well as Flt-1 and p–NF–κB/NF-κB levels, decreased significantly (Fig. 5D–H). The above results illustrated that the exosomes extracted after transfection of miR-144 mimics might alleviate the functional damage of HTR-8/SVneo cells induced by LPS by inhibiting the FosB/Flt-1 pathway.

3.5. *Exos-MSC$^{miR-144}$ might reduce inflammation in pregnant rats with PE-like and improve adverse pregnancy outcomes through the FosB/Flt-1 pathway*

To further verify the above results in animal experiments, a PE-like animal model was constructed. First, low (7.8×10^9 particles/mL), middle (1.55×10^{10} particles/mL), and high concentrations (3.1×10^{10} particles/mL) of exosomes were used to treat LPS-stimulated animals in the model group. The results showed that exosomes at a concentration of 3.1×10^{10} particles/mL significantly inhibited the LPS-stimulated increase in SBP, DBP, and MAP levels. However, treatment with exosomes had no significant effect on heart rate or the urine albumin/creatinine ratio (Figs. S2B–S2C). Therefore, 3.1×10^{10} particles/mL exosomes were chosen as the doses for animal experimental treatments. Then, the animals were injected with exosomes extracted from huc-MSCs under different treatments. The Model + Exos-MSC$^{miR-144}$ group could reverse the LPS-induced reduction in miR-144 expression and increase FosB expression in placental tissue (Fig. 6A and B). The results showed that the levels of systolic and diastolic blood pressure (SBP and DBP), as well as the mean arterial pressure (MAP), in the Model + Exos-MSC^{NC} and Model + Exos-MSC$^{miR-144}$ groups were significantly

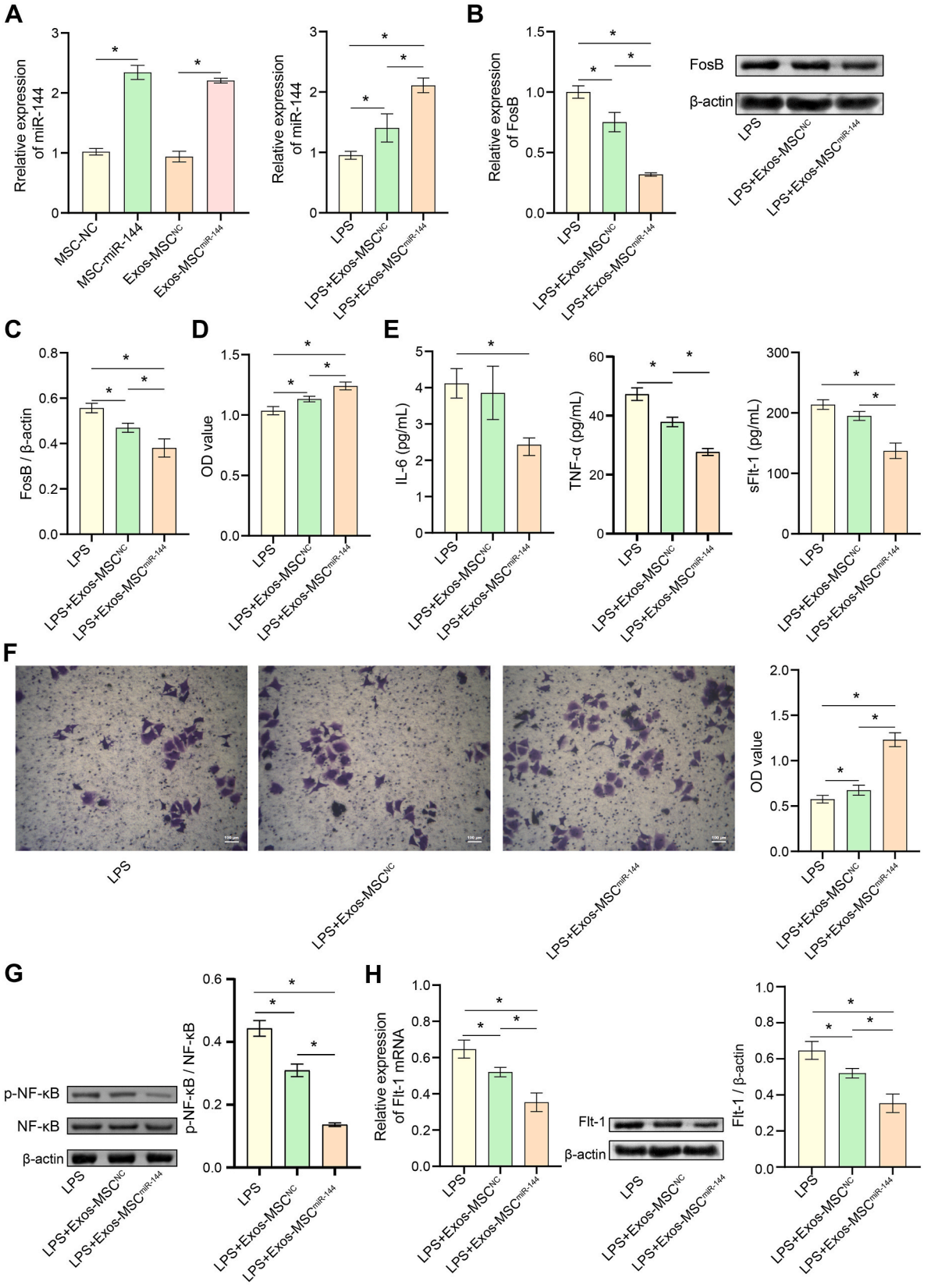

(caption on next page)

Fig. 5. Exos-MSC$^{miR-144}$ might alleviate the functional damage of HTR-8/SVneo cells induced by LPS via inhibiting the FosB/Flt-1 pathway. (A) The expression of miR-144 was detected. (B–C) The expression of FosB was detected by qRT-PCR and Western blot. (D) Cell viability of each group was determined by CCK8. (E) The levels of IL-6, TNF-α, and sFlt-1 were measured by ELISA. (F) Cell migration was assessed by Transwell. (G–H) The Flt-1, p–NF–κB, and NF-κB expressions were measured by qRT-PCR or Western blot. $^*P < 0.05$. n = 3/group. The original immunoblots are available in Fig. S3. Each experiment was repeated at least three times.

lower than those in the Model group, and these levels were lowest in the Model + Exos-MSC$^{miR-144}$ group. Heart rate levels were significantly lower in the Exos-MSC$^{miR-144}$ group than in the model group. However, there was no statistically significant difference in the urine albumin/creatine ratio (Fig. 6C–E). Compared to the Model group, the concentrations of IL-6, TNF-α, and sFlt-1, as well as the Flt-1 and p–NF–κB/NF-κB levels in the serum of pregnant rats in the Model + Exos-MSC^{NC} and Model + Exos-MSC$^{miR-144}$ groups, were decreased. The Model + Exos-MSC$^{miR-144}$ was more obvious (Fig. 6F–I). The above results indicated that Model + Exos-MSC$^{miR-144}$ might reduce inflammation in PE-like pregnant rats through the FosB/Flt-1 pathway.

Next, the pregnancy outcome of pregnant rats was counted. The weight of pregnant rats and live fetuses treated with exosomes accounted for an increase in contrast to the Model group (Fig. 7A and B). The neuronal apoptosis of fetal rats in the Model + Exos-MSC^{NC} and Model + Exos-MSC$^{miR-144}$ groups was less than that in the Model group, and the Model + Exos-MSC$^{miR-144}$ group was more effective (Fig. 7C and D). The Model + Exos-MSC^{NC} and Model + Exos-MSC$^{miR-144}$ groups significantly reduced the LPS-induced rise in the cleaved Caspase3/Caspase3 ratio, and the effect was most pronounced in the Model + Exos-MSC$^{miR-144}$ group (Fig. 7E). The results clarified that Exos-MSC$^{miR-144}$ could improve adverse pregnancy outcomes and alleviate LPS-induced neuronal apoptosis in fetal rat brain tissue.

4. Discussion

In this experiment, we explored the effects of miR-144 or Exos-MSC$^{miR-144}$ on HTR-8/SVneo cells and pregnant rats through the *in vivo* and *in vitro* models stimulated by LPS. In addition, we further explored the effects of Exos-MSC^{NC} and Exos-MSC$^{miR-144}$ on the brain neurons of newborn rats. The study found that Exos-MSC$^{miR-144}$ alleviated gestational hypertension and inflammation in PE-like pregnant rats by regulating the FosB/Flt-1 pathway. In addition, Exos-MSC$^{miR-144}$ might alleviate brain injury in fetal rats.

Clinical data have suggested that plasma LPS levels are significantly elevated in patients with PE compared to those in healthy patients [38]. In general, LPS is a commonly used reagent for modeling inflammation, including PE-like, due to the advantages of easy control, good model reproducibility, and easily identifiable and measurable effects on the whole body. For example, Li et al. established a PE-like rat model by injecting 1.0 μg/kg LPS into the tail vein of normal pregnant rats [31], and Ji et al. investigated the protective effect of cysteine-based peptide in an LPS-induced PE-like rat model [32]. Ma et al. investigated the effect of vitamin D on model rats by an LPS-induced PE-like rat model [39]. Therefore, an LPS-induced PE-like model was used in this study. The results showed that SBP, DBP, MAP, heart rate, urine albumin/creatine ratio, and proinflammatory factor (including IL-6, TNF-α), p–NF–κB/NF-κB, sFlt-1, and Flt-1 levels were significantly increased in rats after LPS induction, suggesting that the model was successfully constructed. We did not explore the role of huc-Exos-MSC in other models, which is a limitation of our study. In future studies, we will explore the role and potential mechanisms of huc-Exos-MSC in other PE models, such as the L-NAME-induced PE model [40].

sFlt1 has become a potential target for the treatment of PE [41]. The concentrations of IL-6, TNF-α and sFlt-1 were increased after LPS treatment [8,42,43]. As an activating protein and transcription factor, AP-1 plays an important role in cancer, immunity, and inflammation [44–46]. However, there are few reports about FosB (AP-1 subunit) in PE. LPS stimulation can directly induce the expression of FosB [8]. The results of the study also showed that HTR-8/SVneo cells induced the expression of FosB and the release of sFlt1 under the LPS stimulation. FosB silencing might alleviate cell inflammation induced by LPS stimulation and improve cell viability and the migration rate. The expression of Flt-1 is related to FosB and c-Fos [47]. The AP-1 pathway might interact with the Flt-1 promoter to regulate the release of sFlt1 [5]. Our results indicated that silencing FosB inhibited Flt-1 expression. The study revealed that silencing FosB to alleviate the symptoms induced by LPS might be related to the inhibition of the Flt-1 pathway.

There are many reports of miRNAs in PE. For example, miR-29a-3p is significantly elevated in PE. Overexpression of miR-29a-3p inhibits hypoxia/reoxygenation-induced endothelial cell viability and angiogenesis [48]. miR-203a-3p inhibits PE inflammation by regulating the expression of IL-24 in macrophages [49]. The current study found that 12 miRNAs (such as miR-144, miR-412–3p, and miR-542–3p) were significantly downregulated and 29 miRNAs were significantly upregulated in the placental tissue of PE. We found that LPS stimulated FosB expression. FosB is one of the main members of the AP-1 family and might be involved in the development of PE [8]. This study focused on exploring the role of crosstalk between miRNAs and FosB in PE. Therefore, bioinformatics analysis was performed to screen for differentially expressed miRNAs that may interact with FosB in PE. We predicted potential miRNAs targeting FosB by dlana tools, such as miR-144, miR-569, and miR-580. The only intersection of miRNAs differentially expressed in PE with potential miRNAs for FosB was miR-144. Therefore, miR-144 was chosen for follow-up studies. Indeed, previous studies have demonstrated that maternal plasma miR-144 is significantly underexpressed in patients with PE [50]. miR-144 expression is downregulated in placental tissues and is involved in the pathogenesis of PE [51]. Consistent with previous studies, further experiments confirmed that miR-144 was downregulated in LPS-induced cells and animal models. It is suggested that downregulation of miR-144 may be a potential biomarker for diagnosing PE. Overexpression of FosB reversed the effects of miR-144 on the inflammation induced by LPS stimulation and the expression of Flt-1. miR-144 targeting FosB has been reported in pancreatic cancer [52]. Dual-luciferase

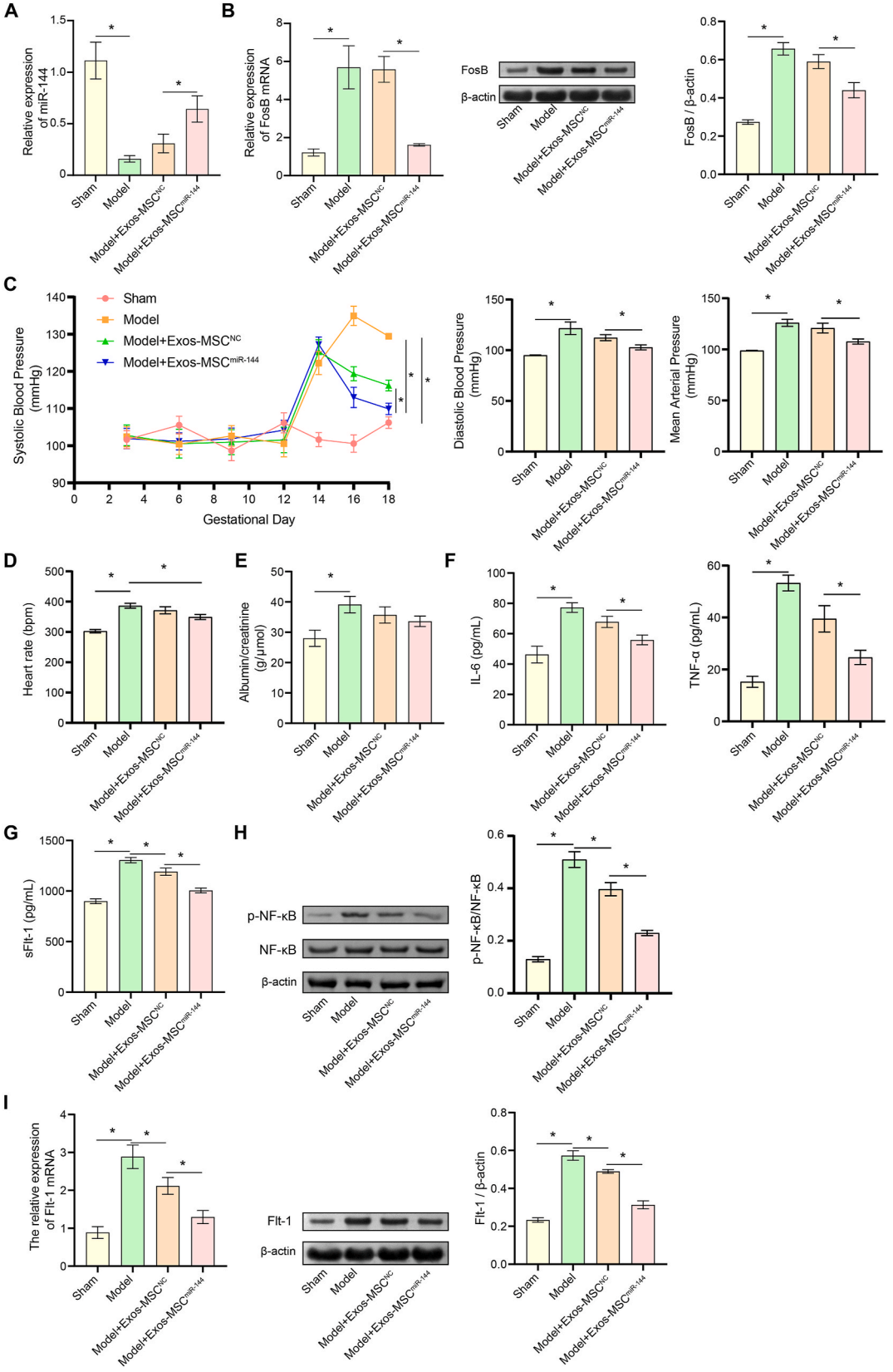

(caption on next page)

Fig. 6. Exos-MSC$^{miR-144}$ might reduce inflammation in PE-like pregnant rats through the FosB/Flt-1 pathway. (A) miR-144 expression in placental tissues was measured by qRT-PCR. (B) FosB expression in placental tissues was detected by qRT-PCR and Western blot. (C–D) SBP, DBP, MAP, and heart rate of pregnant rats during pregnancy were measured. (E) The urine of pregnant rats was collected at GD18 for urine albumin and creatinine. The ratio in the liquid was measured. (F–G) The levels of IL-6, TNF-α, and sFlt-1 were detected by ELISA. (H–I) The levels of Flt-1, p–NF–κB, and NF-κB in the placental tissue were measured by qRT-PCR and Western blot. *$P < 0.05$. n = 10 rats/group. The original immunoblots are available in Fig. S3. Each experiment was repeated at least three times.

confirmed the interaction between FosB and miR-144 in our study. Thus, overexpression of miR-144 might target FosB to reverse the LPS-induced increase in sFlt1 expression and the decrease in cell viability and migration.

EVs derived from hypoxic trophoblast cells regulate chondroitin polymerizing factor by delivering miR-150–3p to inhibit endothelial cell proliferation, migration, and angiogenesis [53]. EVs secreted by trophoblast cells under hypoxic conditions transferred miR-1273d, miR-4492, and miR-4417 to coordinate immune- and inflammation-related pathways to promote PE development [54]. Exos-MSC may alleviate the apoptosis of PE and promote the angiogenesis of placental tissue [16]. In addition, miRNAs derived from Exos-MSC can relieve various diseases, including osteoarthritis, diabetes, and fractures [55–57]. The miRNAs secreted by Exos-MSC are involved in the PE process. For example, the effects of miR-133b and miR-139–5p of Exos-MSC on the PE model have been explored [24,58]. miR-140–5p and miR-342–5p derived from huc-Exos-MSC inhibit the development of PE models [33,59]. As far as we know, the mechanism of action of Exos-MSC$^{miR-144}$ in the PE-like models has been reported for the first time in this subject. Exosomes from the huc-MSCs that overexpressing miR-144 also improved the decrease in cell viability and migration rate caused by LPS stimulation in cell experiments, alleviating the inflammation induced by LPS stimulation. In addition, exosomes from the huc-MSCs that overexpressing miR-144 might alleviate LPS-induced hypertension, urine protein and inflammation in PE-like pregnant rats through the FosB/sFlt1 axis.

The activation of AP-1 is related to the adverse pregnancy outcomes caused by inflammation of the placenta and can affect the survival rate of the offspring [60,61]. In this study, PE-like pregnant rats received a significant increase in the proportion of live births after being injected with Exos-MSC$^{miR-144}$. *In vitro* experiments confirmed that miR-144 and FosB had mutual binding. It is suggested that exosomes might alleviate inflammation in PE-like pregnant rats by targeting FosB via transporting miR-144, thereby improving adverse pregnancy outcomes. The brain nerve development of newborn rats of PE pregnant rats may be affected [62]. AP-1 is associated with LPS-induced neuronal damage [63]. Our results indicated that Exos-MSC$^{miR-144}$ might have a certain alleviating effects on brain neuronal apoptosis in fetal rats. The specific mechanism of action warrants further in-depth study.

Other downregulated miRNAs in maternal PE were not studied, which is a limitation of our study. We plan to verify the effects and potential mechanisms of other miRNAs derived from maternal and huc-MSCs-Exos on PE by RNA sequencing and experiments in future studies. In addition, we focused on the role of FosB in PE, and other subunits of the AP-1 pathway may also play an important role in the process of PE. In the future, it can be further studied.

5. Conclusions

Exos-MSC$^{miR-144}$ alleviated gestational hypertension and inflammation in PE-like pregnant rats by regulating the FosB/Flt-1 pathway. In addition, Exos-MSC$^{miR-144}$ might alleviate brain injury in fetal rats.

Ethics statement

The experiment was approved by the Central South University Animal Welfare Ethics Committee (NO.202103402).

Data availability

Data included in article/supp. material/referenced in article.

Fundings

The research was supported by The Science and Technology Innovation Program of Hunan Province grants (NO·2019SK1010 and 2020SK2072) and the National Key Research and Development Program of China (NO·2016YFC1000206).

CRediT authorship contribution statement

Jingchi Sun: Writing – original draft, Visualization, Formal analysis, Data curation. **Weishe Zhang:** Writing – review & editing, Project administration, Funding acquisition, Conceptualization.

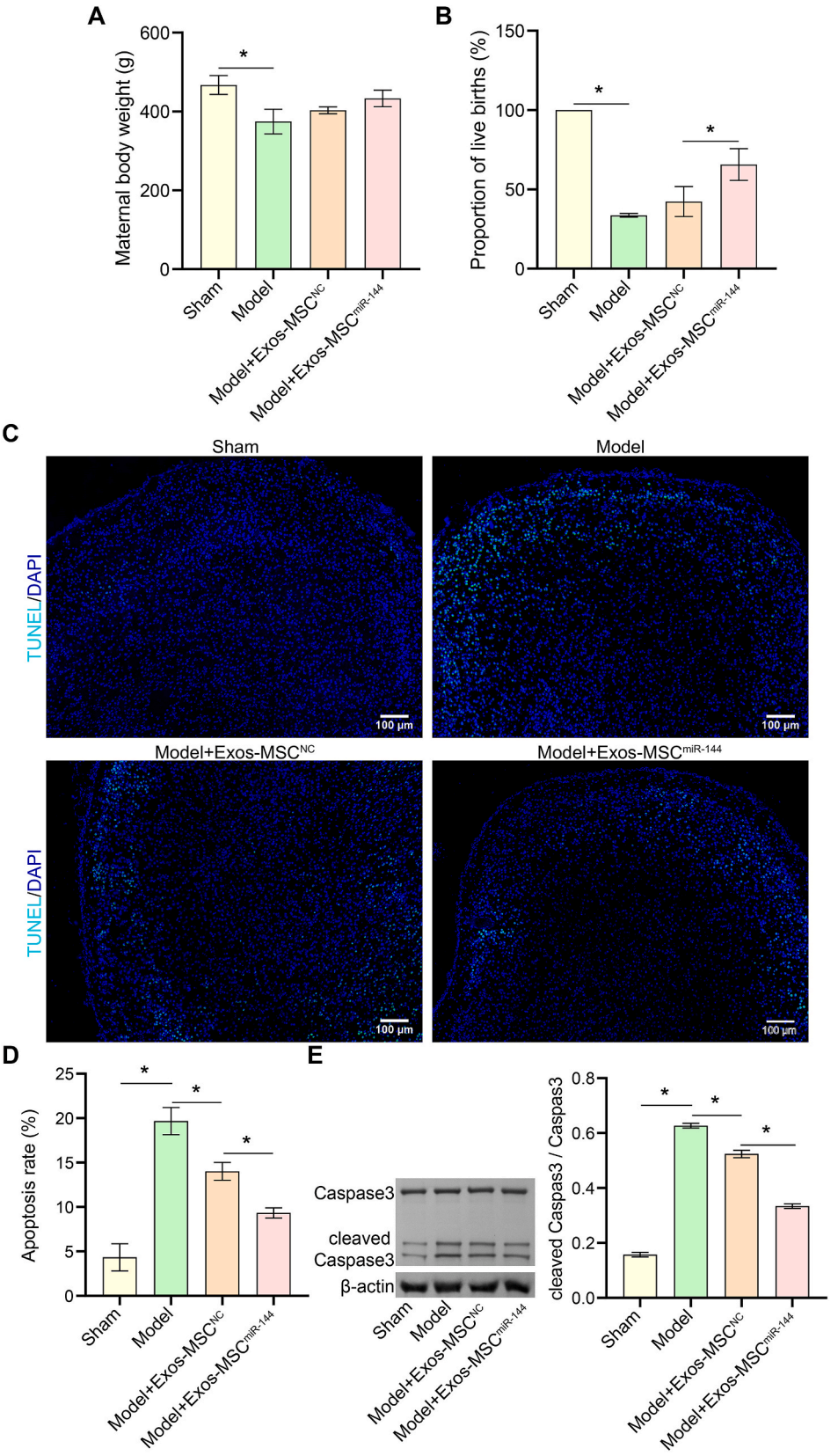

(caption on next page)

Fig. 7. Exos-MSC$^{miR-144}$ improved adverse pregnancy outcomes. (A–B) Statistics on the weight of pregnant rats on GD20 days of pregnancy and the proportion of live births. (C–D) Neuronal apoptosis in fetal rats' brain tissue was measured by TUNEL. The blue color represents nuclei, and the green color represents apoptotic cells. Scale bars: 100 μm (100 ×) or 25 μm (400 ×). (E) cleaved Caspase3 and Caspase3 expressions were measured by Western blot. *$P < 0.05$. n = 10 rats/group. The original immunoblots are available in Fig. S3. Each experiment was repeated at least three times.

Declaration of competing interest

The authors declare that they have no known competing financial interests or personal relationships that could have appeared to influence the work reported in this paper.

The authors declare the following financial interests/personal relationships which may be considered as potential competing interests:Weishe Zhang reports financial support was provided by The Science and Technology Innovation Program of Hunan Province grants. Weishe Zhang reports was provided by National Key Research and Development Program of China.

Appendix A. Supplementary data

Supplementary data to this article can be found online at https://doi.org/10.1016/j.heliyon.2024.e24575.

References

[1] C.W. Ives, R. Sinkey, I. Rajapreyar, A.T.N. Tita, S. Oparil, Preeclampsia-Pathophysiology and clinical presentations: JACC state-of-the-art review, J. Am. Coll. Cardiol. 76 (2020) 1690–1702.
[2] E.A. Phipps, R. Thadhani, T. Benzing, S.A. Karumanchi, Pre-eclampsia: pathogenesis, novel diagnostics and therapies, Nat. Rev. Nephrol. 15 (2019) 275–289.
[3] G.J. Burton, C.W. Redman, J.M. Roberts, A. Moffett, Pre-eclampsia: pathophysiology and clinical implications, Bmj 366 (2019) l2381.
[4] J. Huang, L. Zheng, H. Kong, F. Wang, Y. Su, H. Xin, miR-139-5p promotes the proliferation and invasion of trophoblast cells by targeting sFlt-1 in preeclampsia, Placenta 92 (2020) 37–43.
[5] L. Lin, G. Li, W. Zhang, Y.L. Wang, H. Yang, Low-dose aspirin reduces hypoxia-induced sFlt1 release via the JNK/AP-1 pathway in human trophoblast and endothelial cells, J. Cell. Physiol. 234 (2019) 18928–18941.
[6] S. Lim, W. Li, J. Kemper, A. Nguyen, B.W. Mol, M. Reddy, Biomarkers and the prediction of adverse outcomes in preeclampsia: a systematic review and meta-analysis, Obstet. Gynecol. 137 (2021) 72–81.
[7] S.A. Robertson, Preventing preeclampsia by silencing soluble flt-1? N. Engl. J. Med. 380 (2019) 1080–1082.
[8] P. Xue, W. Fan, Z. Diao, Y. Li, C. Kong, X. Dai, et al., Up-regulation of PTEN via LPS/AP-1/NF-κB pathway inhibits trophoblast invasion contributing to preeclampsia, Mol. Immunol. 118 (2020) 182–190.
[9] A.M. Nuzzo, D. Giuffrida, C. Zenerino, A. Piazzese, E. Olearo, T. Todros, et al., JunB/cyclin-D1 imbalance in placental mesenchymal stromal cells derived from preeclamptic pregnancies with fetal-placental compromise, Placenta 35 (2014) 483–490.
[10] Y. Dai, Z. Diao, H. Sun, R. Li, Z. Qiu, Y. Hu, MicroRNA-155 is involved in the remodelling of human-trophoblast-derived HTR-8/SVneo cells induced by lipopolysaccharides, Hum. Reprod. 26 (2011) 1882–1891.
[11] R.U. Chottekalapanda, S. Kalik, J. Gresack, A. Ayala, M. Gao, W. Wang, et al., AP-1 controls the p11-dependent antidepressant response, Mol. Psychiatr. 25 (2020) 1364–1381.
[12] L. Wang, Y.F. Yang, L. Chen, Z.Q. He, D.Y. Bi, L. Zhang, et al., Compound dihuang granule inhibits nigrostriatal pathway apoptosis in Parkinson's disease by suppressing the JNK/AP-1 pathway, Front. Pharmacol. 12 (2021) 621359.
[13] M. Maqsood, M. Kang, X. Wu, J. Chen, L. Teng, L. Qiu, Adult mesenchymal stem cells and their exosomes: sources, characteristics, and application in regenerative medicine, Life Sci. 256 (2020) 118002.
[14] L. Fu, Y. Liu, D. Zhang, J. Xie, H. Guan, T. Shang, Beneficial effect of human umbilical cord-derived mesenchymal stem cells on an endotoxin-induced rat model of preeclampsia, Exp. Ther. Med. 10 (2015) 1851–1856.
[15] D. Zhang, L. Fu, L. Wang, L. Lin, L. Yu, L. Zhang, et al., Therapeutic benefit of mesenchymal stem cells in pregnant rats with angiotensin receptor agonistic autoantibody-induced hypertension: implications for immunomodulation and cytoprotection, Hypertens. Pregnancy 36 (2017) 247–258.
[16] Z.H. Xiong, J. Wei, M.Q. Lu, M.Y. Jin, H.L. Geng, Protective effect of human umbilical cord mesenchymal stem cell exosomes on preserving the morphology and angiogenesis of placenta in rats with preeclampsia, Biomed. Pharmacother. 105 (2018) 1240–1247.
[17] I. Jaszczuk, D. Koczkodaj, A. Kondracka, A. Kwaśniewska, I. Winkler, A. Filip, The role of miRNA-210 in pre-eclampsia development, Ann. Med. 54 (2022) 1350–1356.
[18] C. Chen, J. Gao, D. Chen, J. Liu, B. He, Y. Chen, et al., miR-4443/MMP2 suppresses the migration and invasion of trophoblasts through the HB-EGF/EGFR pathway in preeclampsia, Cell Cycle 21 (2022) 2517–2532.
[19] H. Zhang, Y. He, J.X. Wang, M.H. Chen, J.J. Xu, M.H. Jiang, et al., miR-30-5p-mediated ferroptosis of trophoblasts is implicated in the pathogenesis of preeclampsia, Redox Biol. 29 (2020) 101402.
[20] G. Qiu, G. Zheng, M. Ge, J. Wang, R. Huang, Q. Shu, et al., Mesenchymal stem cell-derived extracellular vesicles affect disease outcomes via transfer of microRNAs, Stem Cell Res. Ther. 9 (2018) 320.
[21] J. Zhao, X. Li, J. Hu, F. Chen, S. Qiao, X. Sun, et al., Mesenchymal stromal cell-derived exosomes attenuate myocardial ischaemia-reperfusion injury through miR-182-regulated macrophage polarization, Cardiovasc. Res. 115 (2019) 1205–1216.
[22] G. Mao, Z. Zhang, S. Hu, Z. Zhang, Z. Chang, Z. Huang, et al., Exosomes derived from miR-92a-3p-overexpressing human mesenchymal stem cells enhance chondrogenesis and suppress cartilage degradation via targeting WNT5A, Stem Cell Res. Ther. 9 (2018) 247.
[23] X. Cheng, G. Zhang, L. Zhang, Y. Hu, K. Zhang, X. Sun, et al., Mesenchymal stem cells deliver exogenous miR-21 via exosomes to inhibit nucleus pulposus cell apoptosis and reduce intervertebral disc degeneration, J. Cell Mol. Med. 22 (2018) 261–276.
[24] D. Wang, Q. Na, G.Y. Song, L. Wang, Human umbilical cord mesenchymal stem cell-derived exosome-mediated transfer of microRNA-133b boosts trophoblast cell proliferation, migration and invasion in preeclampsia by restricting SGK1, Cell Cycle 19 (2020) 1869–1883.
[25] Q. Yang, S. Zhao, Z. Shi, L. Cao, J. Liu, T. Pan, et al., Chemotherapy-elicited exosomal miR-378a-3p and miR-378d promote breast cancer stemness and chemoresistance via the activation of EZH2/STAT3 signaling, J. Exp. Clin. Cancer Res. 40 (2021) 120.
[26] Y. Liu, L. Lin, R. Zou, C. Wen, Z. Wang, F. Lin, MSC-derived exosomes promote proliferation and inhibit apoptosis of chondrocytes via lncRNA-KLF3-AS1/miR-206/GIT1 axis in osteoarthritis, Cell Cycle 17 (2018) 2411–2422.

[27] X. Gu, Y. Li, K. Chen, X. Wang, Z. Wang, H. Lian, et al., Exosomes derived from umbilical cord mesenchymal stem cells alleviate viral myocarditis through activating AMPK/mTOR-mediated autophagy flux pathway, J. Cell Mol. Med. 24 (2020) 7515–7530.
[28] Y. Wang, X. Du, J. Wang, Transfer of miR-15a-5p by placental exosomes promotes pre-eclampsia progression by regulating PI3K/AKT signaling pathway via CDK1, Mol. Immunol. 128 (2020) 277–286.
[29] B. Mathew, S. Ravindran, X. Liu, L. Torres, M. Chennakesavalu, C.C. Huang, et al., Mesenchymal stem cell-derived extracellular vesicles and retinal ischemia-reperfusion, Biomaterials 197 (2019) 146–160.
[30] D.K. Kim, H. Nishida, S.Y. An, A.K. Shetty, T.J. Bartosh, D.J. Prockop, Chromatographically isolated CD63+CD81+ extracellular vesicles from mesenchymal stromal cells rescue cognitive impairments after TBI, Proc. Natl. Acad. Sci. U. S. A. 113 (2016) 170–175.
[31] Z.H. Li, L.L. Wang, H. Liu, K.P. Muyayalo, X.B. Huang, G. Mor, et al., Galectin-9 alleviates LPS-induced preeclampsia-like impairment in rats via switching decidual macrophage polarization to M2 subtype, Front. Immunol. 9 (2018) 3142.
[32] X. Ji, X. Wang, Z. Ling, Y. Lv, W. Yu, R. Jia, et al., Cys-peptide mediates the protective role in preeclampsia-like rat and cell models, Life Sci. 251 (2020) 117625.
[33] Y. Jiang, T. Luo, Q. Xia, J. Tian, J. Yang, microRNA-140-5p from human umbilical cord mesenchymal stem cells-released exosomes suppresses preeclampsia development, Funct. Integr. Genomics 22 (2022) 813–824.
[34] J. Chen, T. Chen, Y. Zhu, Y. Li, Y. Zhang, Y. Wang, et al., circPTN sponges miR-145-5p/miR-330-5p to promote proliferation and stemness in glioma, J. Exp. Clin. Cancer Res. 38 (2019) 398.
[35] B. Zhang, H.X. Zhang, S.T. Shi, Y.L. Bai, X. Zhe, S.J. Zhang, et al., Interleukin-11 treatment protected against cerebral ischemia/reperfusion injury, Biomed. Pharmacother. 115 (2019) 108816.
[36] Y. Lv, C. Lu, X. Ji, Z. Miao, W. Long, H. Ding, et al., Roles of microRNAs in preeclampsia, J. Cell. Physiol. 234 (2019) 1052–1061.
[37] X. Chang, Q. He, M. Wang, L. Jia, T. Duan, K. Wang, Human Umbilical Cord Mesenchymal Stem Cell (HUCMSC)-derived Exosomes as a Cell-free Therapy for Soluble Fms-like Tyrosine Kinase-1 (Sflt-1)-Induced Endothelial Dysfunction in Preeclampsia, 2021.
[38] J. Wang, X. Gu, J. Yang, Y. Wei, Y. Zhao, Gut microbiota dysbiosis and increased plasma LPS and TMAO levels in patients with preeclampsia, Front. Cell. Infect. Microbiol. 9 (2019) 409.
[39] Y. Ma, Y. Yang, M. Lv, Y. Zhang, Q. He, Y. Zhang, et al., 1,25(OH)(2)D(3) alleviates LPS-induced preeclampsia-like rats impairment in the protective effect by TLR4/NF-kB pathway, Placenta 130 (2022) 34–41.
[40] Y. Li, N. Yang, B. Wang, X. Niu, W. Cai, Y. Li, et al., Effect and mechanism of prophylactic use of tadalafil during pregnancy on l-NAME-induced preeclampsia-like rats, Placenta 99 (2020) 35–44.
[41] A.A. Turanov, A. Lo, M.R. Hassler, A. Makris, A. Ashar-Patel, J.F. Alterman, et al., RNAi modulation of placental sFLT1 for the treatment of preeclampsia, Nat. Biotechnol. (2018).
[42] M. Fan, X. Li, X. Gao, L. Dong, G. Xin, L. Chen, et al., LPS induces preeclampsia-like phenotype in rats and HTR8/SVneo cells dysfunction through TLR4/p38 MAPK pathway, Front. Physiol. 10 (2019) 1030.
[43] A. Yin, Q. Chen, M. Zhong, B. Jia, MicroRNA-138 improves LPS-induced trophoblast dysfunction through targeting RELA and NF-κB signaling, Cell Cycle 20 (2021) 508–521.
[44] N. Feldker, F. Ferrazzi, H. Schuhwerk, S.A. Widholz, K. Guenther, I. Frisch, et al., Genome-wide cooperation of EMT transcription factor ZEB1 with YAP and AP-1 in breast cancer, Embo j 39 (2020) e103209.
[45] M. Yukawa, S. Jagannathan, S. Vallabh, A.V. Kartashov, X. Chen, M.T. Weirauch, et al., AP-1 activity induced by co-stimulation is required for chromatin opening during T cell activation, J. Exp. Med. (2020) 217.
[46] L. Subedi, J.H. Lee, S. Yumnam, E. Ji, S.Y. Kim, Anti-inflammatory effect of sulforaphane on LPS-activated microglia potentially through JNK/AP-1/NF-κB inhibition and Nrf 2/HO-1 activation, Cells 8 (2019).
[47] D.I. Holmes, I. Zachary, Placental growth factor induces FosB and c-Fos gene expression via Flt-1 receptors, FEBS Lett. 557 (2004) 93–98.
[48] Z. Liu, N. Guo, X.J. Zhang, Long noncoding TUG1 promotes angiogenesis of HUVECs in PE via regulating the miR-29a-3p/VEGFA and Ang 2/Tie 2 pathways, Microvasc. Res. 139 (2022) 104231.
[49] H.Y. Ma, W. Cu, Y.H. Sun, X. Chen, MiRNA-203a-3p inhibits inflammatory response in preeclampsia through regulating IL24, Eur. Rev. Med. Pharmacol. Sci. 24 (2020) 5223–5230.
[50] H. Li, Q. Ge, L. Guo, Z. Lu, Maternal plasma miRNAs expression in preeclamptic pregnancies, BioMed Res. Int. 2013 (2013) 970265.
[51] S. Hu, J. Li, M. Tong, Q. Li, Y. Chen, H. Lu, et al., MicroRNA-144-3p may participate in the pathogenesis of preeclampsia by targeting Cox-2, Mol. Med. Rep. 19 (2019) 4655–4662.
[52] S. Liu, J. Luan, Y. Ding, miR-144-3p targets FosB proto-oncogene, AP-1 transcription factor subunit (FOSB) to suppress proliferation, migration, and invasion of PANC-1 pancreatic cancer cells, Oncol. Res. 26 (2018) 683–690.
[53] M. Sha, S. Zhang, R. Beejadhursing, Y. Sun, Y. Qin, S. Chen, et al., Extracellular vesicles derived from hypoxic HTR-8/SVneo trophoblast inhibit endothelial cell functions through the miR-150-3p/CHPF pathway, Placenta 138 (2023) 21–32.
[54] L. Li, X. Li, Y. Zhu, L. Li, Y. Wu, J. Ying, et al., Human trophoblast cell-derived extracellular vesicles facilitate preeclampsia by transmitting miR-1273d, miR-4492, and miR-4417 to target HLA-G, Reprod. Sci. 29 (2022) 2685–2696.
[55] W. Liu, L. Li, Y. Rong, D. Qian, J. Chen, Z. Zhou, et al., Hypoxic mesenchymal stem cell-derived exosomes promote bone fracture healing by the transfer of miR-126, Acta Biomater. 103 (2020) 196–212.
[56] J. Wu, L. Kuang, C. Chen, J. Yang, W.N. Zeng, T. Li, et al., miR-100-5p-abundant exosomes derived from infrapatellar fat pad MSCs protect articular cartilage and ameliorate gait abnormalities via inhibition of mTOR in osteoarthritis, Biomaterials 206 (2019) 87–100.
[57] M. Yu, W. Liu, J. Li, J. Lu, H. Lu, W. Jia, et al., Exosomes derived from atorvastatin-pretreated MSC accelerate diabetic wound repair by enhancing angiogenesis via AKT/eNOS pathway, Stem Cell Res. Ther. 11 (2020) 350.
[58] H. Liu, F. Wang, Y. Zhang, Y. Xing, Q. Wang, Exosomal microRNA-139-5p from mesenchymal stem cells accelerates trophoblast cell invasion and migration by motivation of the ERK/MMP-2 pathway via downregulation of protein tyrosine phosphatase, J. Obstet. Gynaecol. Res. 46 (2020) 2561–2572.
[59] Y. Chen, J. Jin, X. Chen, J. Xu, L. An, H. Ruan, Exosomal microRNA-342-5p from human umbilical cord mesenchymal stem cells inhibits preeclampsia in rats, Funct. Integr. Genomics 23 (2023) 27.
[60] L. Chen, H. Wu, L. Le, P. Yang, F. Fu, W. Liu, et al., Exposure to silver nanoparticles induces immunological dysfunction in pregnant mice, Environ. Toxicol. 35 (2020) 1161–1169.
[61] X. Lin, Q. Peng, J. Zhang, X. Li, J. Huang, S. Duan, et al., Quercetin prevents lipopolysaccharide-induced experimental preterm labor in mice and increases offspring survival rate, Reprod. Sci. 27 (2020) 1047–1057.
[62] H. Cosar, E. Ozer, H. Topel, Z. Kahramaner, E. Turkoglu, A. Erdemir, et al., Neuronal apoptosis in the neonates born to preeclamptic mothers, J. Matern. Fetal Neonatal Med. 26 (2013) 1143–1146.
[63] G.W. Jeong, H.H. Lee, W. Lee-Kwon, H.M. Kwon, Microglial TonEBP mediates LPS-induced inflammation and memory loss as transcriptional cofactor for NF-κB and AP-1, J. Neuroinflammation 17 (2020) 372.